Dermaseptin S9, an α-Helical Antimicrobial Peptide with a Hydrophobic Core and Cationic Termini†

Olivier Lequin,‡ Ali Ladram,§ Ludovic Chabbert,‡ Francine Bruston,§ Odile Convert,‡ Damien Vanhoye,§ Gérard Chassaing,‡ Pierre Nicolas,§ and Mohamed Amiche*,§

Peptidome de la peau d'amphibiens, FRE 2852, CNRS-Université Paris 6, Tour 43, Institut Jacques Monod, 2 Place Jussieu, 75251 Paris Cedex 05, France, and Synthèse, structure et fonction de molécules bioactives, UMR 7613 CNRS, Université Pierre et Marie Curie, Case Courrier 45, 4 Place Jussieu, 75252 Paris Cedex 05, France, and Peptidome de la peau d'amphibiens, FRE 2852 CNRS, Université Pierre et Marie Curie, Tour 43, Institut Jacques Monod, 2 Place Jussieu, 75251 Paris Cedex 05, France

Received August 26, 2005; Revised Manuscript Received October 27, 2005

ABSTRACT: The dermaseptins S are closely related peptides with broad-spectrum antibacterial activity that are produced by the skin of the South American hylid frog, *Phyllomedusa sauvagei*. These peptides are polycationic (Lys-rich), α-helical, and amphipathic, with their polar/charged and apolar amino acids on opposing faces along the long axis of the helix cylinder. The amphipathic α-helical structure is believed to enable the peptides to interact with membrane bilayers, leading to permeation and disruption of the target cell. We have identified new members of the dermaseptin S family that do not resemble any of the naturally occurring antimicrobial peptides characterized to date. One of these peptides, designated dermaseptin S9, GLRSKIWLWVLLMIWQESNKFKKM, has a tripartite structure that includes a hydrophobic core sequence encompassing residues 6−15 (mean hydrophobicity, +4.40, determined by the Liu−Deber scale) flanked at both termini by cationic and polar residues. This structure is reminiscent of that of synthetic peptides originally designed as transmembrane mimetic models and that spontaneously become inserted into membranes [Liu, L., and Deber, C. M. (1998) *Biopolymers 47,* 41−62]. Dermaseptin S9 is a potent antibacterial, acting on Gram-positive and Gram-negative bacteria. The structure of dermaseptin S9 in aqueous solution and in TFE/water mixtures was analyzed by circular dichroism and two-dimensional NMR spectroscopy combined with molecular dynamics calculations. Dermaseptin S9 is aggregated in water, but a monomeric nonamphipathic α-helical conformation, mostly in residues 6−21, is stabilized by the addition of TFE. These results, combined with membrane permeabilization assays and surface plasmon resonance analysis of the peptide binding to zwitterionic and anionic phospholipid bilayers, demonstrate that spatial segregation of hydrophobic and hydrophilic/charged residues on opposing faces along the long axis of a helix is not essential for the antimicrobial activity of cationic α-helical peptides.

The amphipathic α helix is a common motif found in many cell lytic peptides including cationic antimicrobial peptides that help defend eukaryotes against invading microorganisms (*1*−*11*). Linear antimicrobial peptides are classified according to their primary structure (*11*−*17*), but they all, regardless of their length or amino acid sequence, form an amphipathic α helix when bound to lipid bilayers, with their polar and apolar amino acids on opposing surfaces along the long axis of the helix. The importance of amphipathic helices for mediating lipid−protein interactions was first recognized by Segrest et al. (*18*). This structural element is now believed to play a crucial role in the binding of cationic host-defense peptides to the negatively charged outer leaflet of bacterial bilayers. Once bound, the hydrophobic face of the amphipathic peptide would then permit the peptide to enter the membrane interior, thereby triggering local fusion of the membrane leaflets, pore formation, cracks, and membrane disruption (*19*−*23*). Because they do not interact stereospecifically with a membrane receptor, cationic antimicrobial peptides that form an amphipathic α helix can accumulate and accommodate several mutations without the loss of efficacy, as long as their amino acid sequences satisfy the criteria of appropriate cationicity, amphipathicity, and helical propensity. Altough there is a correlation between the activities, helicity, and amphipathicity in host-defense peptides (*24*−*37*), recent studies have shown that significantly altering the amphipathic structure of a synthetic helical lytic peptide by reshuffling its sequence did not affect the antimicrobial activity of the peptides (*38*). However, a pronounced effect was observed regarding their hemolytic activity and their ability to bind the zwitterionic membrane. This raises the question of whether an amphipathic structure is a fundamental requirement for the binding of α-helical antimicrobial peptides to anionic membranes and their permeation/disruption.

Frog skin is a particularly rich source of antimicrobial peptides, including α-helical antimicrobial peptides (*11*−

† This work was supported by the CNRS and the "Programme de Recherche Fondamentale en Microbiologie et Maladies Infectieuses et Parasitaires (PRFMMIP)".

* To whom correspondence should be addressed: FRE 2852, CNRS-Université Paris 6, Tour 43, Institut Jacques Monod, 2 Place Jussieu, 75251 Paris Cedex 05, France. Telephone: 33-1-44-27-69-52. Fax: 33-1-44-27-59-94. E-mail: pnicolas@ccr.jussieu.fr (P.N.); amiche@ccr.jussieu.fr (M.A.).

‡ UMR 7613, Université Pierre et Marie Curie.

§ FRE 2852, Université Pierre et Marie Curie.

10.1021/bi051711i CCC: $33.50
Published on Web 12/14/2005

Table 1: Comparison of the Amino Acid Sequences of Dermaseptins S from *P. sauvagei*

Dermaseptin	S1[a, b, c]	ALWKTMLKKLG-TMALHAGKAALGAAADTISQ--GTQ
Dermaseptin	S2[a]	ALWFTMLKKLG-TMALHAGKAALGAAANTISQ--GTQ
Dermaseptin	S3[a]	ALWKNMLKGIGK----LAGKAALGAVKKLVGAES---
Dermaseptin	S4[a]	ALWMTLLKKVLK----AAAKAALNAV--LVGANA---
Dermaseptin	S5[a]	GLW-SKIKTAGKSVAKAAAKAAVKAVTNAV-------
Dermaseptin	S6[b]	GLW-SKIKTAGKEAAKAAAKAAGKAALNAVSEAIgEQ
Dermaseptin	S7[b]	GLWKSLLKNVGK----AAGKAALNAVTDMVNQ--gEQ
Dermaseptin	S8[b]	ALWKTMLKKLG-TVALHAGKAALGAAADTISQ--gAQ
Dermaseptin	S11[c]	ALWKTLLKGAGKVFGHVA-KQFLG------SQGQPES
Dermaseptin	S12[c]	GLW-SKIKEAAKT----AGKMAMGWVNDMV----gEQ
Dermaseptin	S13[c]	GL-RSKIKEAAKT----AGKMALGWVNDMA----gEQ
Dermaseptin	S10[c]	GLVSDLLSTVTG----LLGNLGGGGLKKI--------
Dermaseptin	S9[c]	GL-RSKIWLWVLLMIWQESNKFKKM----------

Alignments were performed by using CLUSTAL X Multiple Sequence Alignment software (*81*). Gaps (−) have been introduced to maximize sequence similarities. Identical amino acids have shaded backgrounds. Similar amino acids are in bold. Amino acids in italic are removed during processing of proforms to expose the extra Gly residue (lowercase letters), which serves as an amide donor for the C-terminal residue of mature peptides. The amino acid sequence is in the standard one-letter code. [a] From ref *40*. [b] From ref *41*. [c] Sequences predicted from cDNA clones in this study (EMBL Nucleotide Sequence Database accession numbers: dermaseptins S9−S11, AJ972905, AJ972906, AJ972907, AJ972908, AJ972909, and AJ972909).

16). Many studies have shown that a given species of frog produces many structurally related isoforms of α-helical antimicrobial peptides that differ by only a few amino acid substitutions and/or deletions. Each isoform may have a specific spectrum of activity against a range of microorganisms. It has been speculated that the diversification of antimicrobial peptides within a species is part of an evolutionary strategy for providing frogs with the maximum protection against a wide range of microorganisms (*14*, *39*). Thus, studies on the evolution and diversity of frog skin antimicrobial peptides may help reveal new peptides targeting specific microorganisms against which few therapeutic armaments are available. The discovery of new isoforms with novel structural and biochemical properties may also shed light on the exact roles of various parameters, such as charge, degree of helical structure, amphipathy, and flexibility, on the ability of helical peptides to bind to and disrupt bacterial membranes.

The dermaseptins S form a family of eight closely related amphipathic α-helical peptides from frog skin that all have a conserved Trp residue at position 3, an AG(A)KAAL(V/G)G(N/K)AV(A) consensus motif in the mid-region, and a positive charge attributable to the presence of Lys residues that punctuate an alternating hydrophobic and hydrophilic sequence (*40*, *41*). The peptides have 30−94% sequence identity (Table 1) and exhibit broad-spectrum antibacterial activities, at micromolar concentrations, against Gram-positive and Gram-negative bacteria, although their specificities overlap widely and their potencies differ markedly. The dermaseptins S are all derived from a single family of precursor polypeptides that have a characteristic tripartite organization, including a remarkably well-conserved signal peptide, a conserved acidic propiece that ends in a typical prohormone processing signal (Lys-Arg), and a variable dermaseptin S-encoding region (*42*). We have used the conservation of the preproregion sequences of the prepro-dermaseptin transcripts to identify five new members of the dermaseptins S family in the South American hylid frog *Phyllomedusa sauvagei* (subfamily: Phyllomedusinae). One of these peptides, dermaseptin S9, is potent against Gram-positive and Gram-negative bacteria but does not resemble any antimicrobial peptide identified to date. It is more similar to the synthetic peptides that were originally designated as transmembrane mimetic model peptides (*43*−*45*), having a hydrophobic core sequence flanked at both termini by several positively charged residues. These peptides become inserted into membranes, provided that the average hydrophobicity of their core segment is above an experimentally determined threshold value based on the Liu−Deber hydrophobicity scale (*44*, *45*). Our analyses indicate that dermaseptin S9 folds into an α helix in structure-promoting solvents and binds to and permeates membranes. Thus, segregation of polar/charged and apolar amino acids on opposing faces along the long axis of the helix cylinder does not seem to be required for the antimicrobial activity of cationic α-helical peptides.

MATERIALS AND METHODS

Frog Species. Specimens of *P. sauvagei* were obtained from "La Ferme Tropicale" (Paris, France). They were housed in large wooden cages (120 × 90 × 90 cm), covered on three sides by plastic mosquito netting (*46*). Philloden-dron, Potos, and Dracena were used as perches, and water bowls were provided for nocturnal bathing. The frogs were fed crickets.

cDNA Cloning. cDNAs were cloned using the technique developed by Shaw et al. (*41*), by which amphibian skin peptide precursors can be cloned from libraries constructed from lyophilized skin secretions or freshly collected skin exudates without killing the animals. Briefly, 200 μL samples of skin exudate were dissolved in 1 mL of cell lysis/mRNA stabilization solution (Dynal, U.K.). Polyadenylated mRNA was isolated using magnetic oligo-dT beads (Dynal Biotech, U.K.). The cDNA was synthesized by RT-polymerase chain reaction (PCR),[1] with 3′ rapid amplification of cDNA ends (RACE) (Invitrogen) using a 5′ primer (5′-GGCTTCCCT-GAAGAAATCTC-3′) corresponding to the nucleotide sequence encoding the conserved N terminus of the prepro-region of dermaseptin precursors (*47*) and a primer specific to the 3′ adaptator under the following conditions: 35 cycles of 94 °C for 240 s, 56 °C for 45 s, and 72 °C for 60 s and 1 cycle of 72 °C for 10 min. The PCR product was cloned into the pGEMt-easy vector system (Promega) using standard procedures (*48*) and used to transform competent JM 109 *Escherichia coli*. The white positive colonies of transformed

E. coli were screened with T7 (5′-ATTATGCTGAGTGATACCCGCT-3′) and SP6 (5-ATTTAGGTGACACTATAGAATAC-3′) primers. Amplification products of the expected sizes (400−500 bp) were sequenced by the dideoxy chain terminator method.

Solid-Phase Peptide Synthesis. Dermaseptin S9 and dermaseptin B2 were synthesized using solid-phase FastMoc chemistry procedures on an Applied Biosystems 433A automated peptide synthesizer. The peptidylresin and side-chain protection bonds were cleaved by incubation in a mixture of 95% trifluoroacetic acid (TFA), 2.5% triisopropylsilane, and 2.5% water for 2 h at room temperature. The resulting mixture was filtered to remove the resin, and the crude peptides were precipitated with ether at −20 °C. They were recovered by centrifugation at 5000*g* for 15 min at 4 °C, washed 3 times with cold ether, dried under a stream of nitrogen, dissolved in 10% acetic acid, and lyophilized. The crude peptides were purified by reverse-phase high-performance liquid chromatography (HPLC), and the homogeneity and identity of the peptides were assessed by MALDI−TOF mass spectrometry (Voyager DE RP, Perseptive Biosystems) and analytical HPLC as described (*49*).

Antimicrobial Assays. Gram-positive eubacteria (*Bacillus megaterium*, *Listeria monocytogenes*, *Staphylococcus aureus*, and *Staphylococcus haemolyticus*) and Gram-negative eubacteria (*E. coli* 363, *Salmonella typhimurium*, and *Klebsiella pneumoniae*) were cultured as described previously (*49*). The minimal inhibitory concentrations (MICs) of peptides were determined in 96-well microtitration plates by growing the bacteria in the presence of 2-fold serial dilutions of peptide. Aliquots (10 μL) of each serial dilution were incubated for 16 h at 37 °C with 100 μL of a suspension of a midlogarithmic phase culture of bacteria at a starting absorbance A_{630} = 0.001 in Poor-Broth nutrient medium (1% bactotryptone and 0.5% NaCl, w/v). Inhibition of growth was assayed by measuring the absorbance at 630 nm. The MIC was defined as the lowest concentration of peptide that inhibited the growth of ≥99% of the cells. Bacteria were incubated for 2 h with different concentrations of peptides and plated out on solid culture medium containing 1% noble agar to distinguish between bacteriostatic and bactericidal effects. The plates were subsequently incubated and examined daily for the formation of colonies. All assays were performed in triplicate plus positive controls without the peptide and negative controls with 0.7% formaldehyde.

Hemolysis of Rat Red Blood Cells. The hemolytic activity of the peptides was determined using fresh rat erythrocytes. The blood was centrifuged, and the erythrocytes were rinsed 3 times with PBS (35 mM phosphate buffer and 0.15 M NaCl at pH 7.4). Peptides were incubated with the erythrocyte suspension (4% erythrocytes, v/v, in PBS) at 37 °C for 60 min, and the erythrocytes were removed by centrifugation at 800*g* for 10 min. Hemolysis was assessed by measuring the optical density at 540 nm of the supernatant. Erythrocytes lysed with 1% Triton X-100 were used as a standard for 100% hemolysis.

Peptide-Induced Permeabilization of the Cytoplasmic Membrane of E. coli. The permeabilization of the cytoplasmic membrane of *E. coli* 363 by dermaseptin S9 and dermaseptin B2 was assayed by measuring the β-galactosidase activity with the chromogenic substrate *o*-nitrophenyl-β-D-galactopyranoside (ONPG). *E. coli* 363 was grown in 10% Luria−Bertani broth in the presence of 100 μg/mL IPTG (Sigma) to induce the enzyme. Bacteria were washed twice with 10% LB in PBS (0.15 M phosphate and 0.2 M NaCl at pH 7.4) and diluted to an A_{630} of 0.5 in 10% LB in PBS. Aliquots (50 μL) of bacterial suspension were then mixed with 2 mM ONPG and incubated with the peptide (3 μM). The hydrolysis of ONPG was monitored by measuring the absorbance at 420 nm of released *o*-nitrophenol. Complete permeabilization was assessed using sonicated bacteria. All of the results are the means of 3−5 independent experiments.

Circular Dichroism (CD) Spectroscopy. The CD spectra of the peptides were recorded with a Jasco J-810 CD spectropolarimeter (Jasco Corp., Tokyo, Japan) linked to a PC microprocessor. The instrument outputs were calibrated with D(+)-10-camphorsulfonic acid. The spectra were scanned at 25 °C in a quartz optical cell with a 1 mm path length. Spectral measurements were obtained at wavelengths of 190−250 nm, at a scan rate of 20 nm/min with a bandwidth of 1 nm. Typically, five scans were accumulated and averaged. The CD spectrum of each peptide was measured in 0.05 M phosphate buffer (pH 7) and in the presence of increasing concentrations of TFE; the peptide concentration was 20 μM. The CD spectrum of the buffer and/or TFE solutions without the peptide was used as baseline. CD measurements are reported as $\Delta\epsilon$ (M^{-1} cm^{-1}). The relative helix content was deduced according to Zhong and Johnson (*50*) as the percent helix = $-[\Delta\epsilon_{222\ nm} \times 10]/n$, where $\Delta\epsilon_{222\ nm}$ is the dichroic increment at 222 nm and n is the number of residues in the peptide.

Preparation of Large Unilamellar Vesicles (LUVs). 1,2-Dimyristoyl-*sn*-glycero-3-phosphatidylcholine (DMPC) and DMPG were purchased from Avanti Polar Lipids. Phospholipid vesicles were prepared by extrusion, and their average diameter (100 ± 20 nm) was estimated by turbidity at 436 nm using a 1 cm path-length cuvette (*51*). Briefly, dry DMPC or DMPG (30 mg) were dissolved in chloroform. The solvent was evaporated under a stream of nitrogen, and the lipids were held under a vacuum for 20 min. The dried lipids were hydrated by vortexing and/or sonicating in 50 mM phosphate buffer (pH 7) plus 150 mM NaCl. The resultant lipid dispersion (14 mM with respect to phospholipids) was extruded 11 times through decreasing pore-size filters (from 800 to 100 nm) to obtain 100 nm LUVs. They were stored at 4 °C.

Binding Analysis by Surface Plasmon Resonance (SPR) Biosensor. Biosensor experiments were carried out at 25 °C with a Biacore 2000 biosensor (Biacore, Uppsala, Sweden) using L1 sensor chips (BIAcore). PBS (50 mM phosphate buffer at pH 7 plus 150 mM NaCl) was the running buffer. All solutions were degassed and filtered through a 0.22 μm

[1] Abbreviations: CD, circular dichroism; CSD, chemical-shift deviation; DMPC, 1,2-dimyristoyl-*sn*-glycero-3-phosphatidylcholine; DQF-COSY, double-quantum-filtered correlation spectroscopy; DRP, dermaseptin-related peptide; DRS, dermaseptin; HPLC, high-performance liquid chromatography; HSQC, heteronuclear single-quantum correlation; LUV, large unilamellar vesicle; MIC, minimal inhibitory concentration; NMR, nuclear magnetic resonance; NOE, nuclear Overhauser effect; ONPG, *o*-nitrophenyl-β-D-galactopyranoside; NOESY, NOE spectroscopy; PCR, polymerase chain reaction; RACE, rapid amplification of cDNA ends; SPR, surface plasmon resonance; TFA, trifluoroacetic acid; TFE, trifluoroethanol; TOCSY, total correlation spectroscopy.

filter. The L1 sensor chip contains hydrophobic aliphatic chains covalently linked to a dextran-coated gold surface. DMPC or DMPG LUVs (60 μL, 0.5 mM in 50 mM phosphate buffer at pH 7 plus 150 mM NaCl) were run onto the sensor chip (2 μL/min). The liposomes were captured on the surface of the sensor chip by the lipophilic compounds to produce a supported lipid bilayer. Multilamellar structures were removed by injecting a brief pulse (12 s) of 100 mM NaOH. Peptide solutions (60 μL of peptide in PBS, 180 s) were injected onto the bilayer surface at 20 μL/min to avoid limitation by mass transport. The peptide solution was then replaced by PBS, and the peptide−bilayer complex was allowed to dissociate for 180 s. The biosensor chip surface was regenerated by removing the bound phospholipids with an injection of 40 mM *n*-octyl-D-glucopyranoside (100 μL, 10 μL/min). The SPR response (a change in resonance signal), expressed as RU, depends upon the density of the peptide adsorbed onto the membrane. The affinity of the peptide for lipids was estimated from a series of response curves. The resulting sensorgrams were collected for several concentrations of each peptide interacting with each lipid surface. The peptide−lipid interaction sensorgrams were analyzed by curve fitting using numerical integration analysis (see below). Data were fitted globally by simultaneous fitting of the peptide sensorgrams obtained at various concentrations from 1.25 to 40 μM. Three methods are currently used to calculate kinetic rate constants from biosensor data: linearization, curve fitting with analytical integration, and curve fitting with numerical integration. Linearization can be used to estimate the rate constants when the analyte A binds to immobilized ligand B in a simple bimolecular or Langmuir interaction. However, our experimental sensorgrams do not fit the simple bimolecular model (see the Results). This may be the result of steric hindrance or a more complex interaction. Because a poor fit was obtained with the simple 1:1 binding model, the two-state reaction model was used to determine the association and dissociation rate constants

$$P + L \leftrightarrow PL \leftrightarrow PL^*$$

where peptide (P) binds to lipids (L) to give the complex PL (primary binding). PL subsequently changes to PL*, which represents the penetration of the peptide into the hydrophobic core of the bilayer. PL* cannot dissociate directly to P and L. The rate constants and equilibrium affinity constants of each steps were determined by BIA biospecific interaction analysis using the BIA evaluation and BIA simulation software.

Nuclear Magnetic Resonance (NMR) Spectroscopy. NMR samples were prepared in TFE-d_3/H_2O/D_2O (30:72:8, v/v/v); the dermaseptin S9 concentration was 2 mM. Sodium 3-(trimethylsilyl)-propionate-2,2,3,3-d_4 was used as an internal reference for chemical-shift calibration. NMR spectra were recorded on Bruker Avance spectrometers operating at a ^{1}H frequency of 500 MHz and were processed with Bruker XWINNMR software. One-dimensional spectra were acquired over 4000 data points using a spectral width of 6000 Hz. Solvent resonance was suppressed by presaturation during the relaxation delay (1−1.5 s) or with a WATERGATE sequence using pulsed field gradients (*52*). Proton assignments were obtained from the analysis of 2D total correlation spectroscopy (TOCSY) (clean MLEV-17 isotropic scheme of 20−85 ms duration) (*53*, *54*), NOE spectroscopy (NOESY) (waterflipback pulse, mixing times of 100 and 200 ms) (*55*, *56*), double-quantum-filtered correlation spectroscopy (DQF-COSY) (*57*), and ^{1}H-^{13}C heteronuclear single-quantum correlation (HSQC) spectra (*58*). Homonuclear 2D experiments were acquired in phase-sensitive mode using States-TPPI quadrature mode, with the transmitter set on the solvent signal. Two-dimensional data were typically collected with 360−512 t_1 increments and 2048 data points in t_2, over a spectral width of 6000 Hz in both dimensions. The time domain data were multiplied by 60−90° shifted sine-bell functions and zero-filled prior to Fourier transformation in t_2 and t_1. Baseline distortions were corrected with a fifth-order polynomial function. Spectra were analyzed with the aid of XEASY (*59*). The chemical-shift deviations (CSDs) of H^α protons were calculated using the set of random-coil values reported in water. $^3J_{H^N-H^\alpha}$ coupling constants were extracted with INFIT (*60*) from a 2D NOESY spectrum recorded with a long acquisition time in the t_2 dimension (340 ms).

NMR Restraints. Interproton distance restraints were derived from a 2D NOESY spectrum recorded with a 100 ms mixing time. NOESY cross-peaks were integrated using XEASY, and peak volumes were converted into upper distance bounds using the calibration routine in DYANA (*61*). The lower bounds were set to the sum of the van der Waals radii of two protons (1.8 Å). Pseudoatoms were introduced for distances involving equivalent protons, and upper limits were corrected appropriately (*62*). The constraints on the backbone ϕ torsion angle were determined from the analysis of intraresidual $d\alpha$N NOE and $^3J_{H^N-H^\alpha}$ coupling constants. The ϕ torsion angle was restrained to negative values for non-glycine residues, which showed no strong intraresidual $d\alpha$N NOE (*63*), and was further restrained to [−90°, −30°] for residues exhibing a $^3J_{H^N-H^\alpha}$ coupling constant lower than 6 Hz. The χ_1 torsion angle of three residues could be restrained from the analysis of intraresidual $d\beta$N NOEs and from the measurement of $^3J_{H^\alpha-H\beta}$ coupling constants on a 2D DQF-COSY spectrum.

Structure Calculations. Structures were calculated using DYANA (*61*) and XPLOR-NIH (*64*) running on SGI O2 R10000 workstations. A set of 100 structures was generated by torsion-angle dynamics in DYANA using a standard simulated annealing protocol (*61*). The best 20 structures were then subjected to conjugate-gradient minimization within XPLOR-NIH using the CHARMM22 force field. The nonbonded interactions were calculated with a 12 Å cutoff, using a Lennard−Jones potential for the van der Waals term and a distance-dependent dielectric function ($\epsilon = 4r$) for the electrostatic energy. Structures were visualized using InsightII version 98 (Accelrys, Inc., San Diego, CA). The structure quality was assessed with PROCHECK-NMR (*65*).

RESULTS

cDNA Cloning of Preprodermaseptins S from P. sauvagei. 3′ RACE analysis of skin mRNA from *P. sauvagei* using a primer corresponding to the nucleotide sequence encoding the conserved N terminus of the preproregion of dermaseptin precursors revealed six different cDNAs encoding 69−80 residue sequences starting with a Met codon and ending with a stop codon (Figure 1A). The deduced amino acid sequences

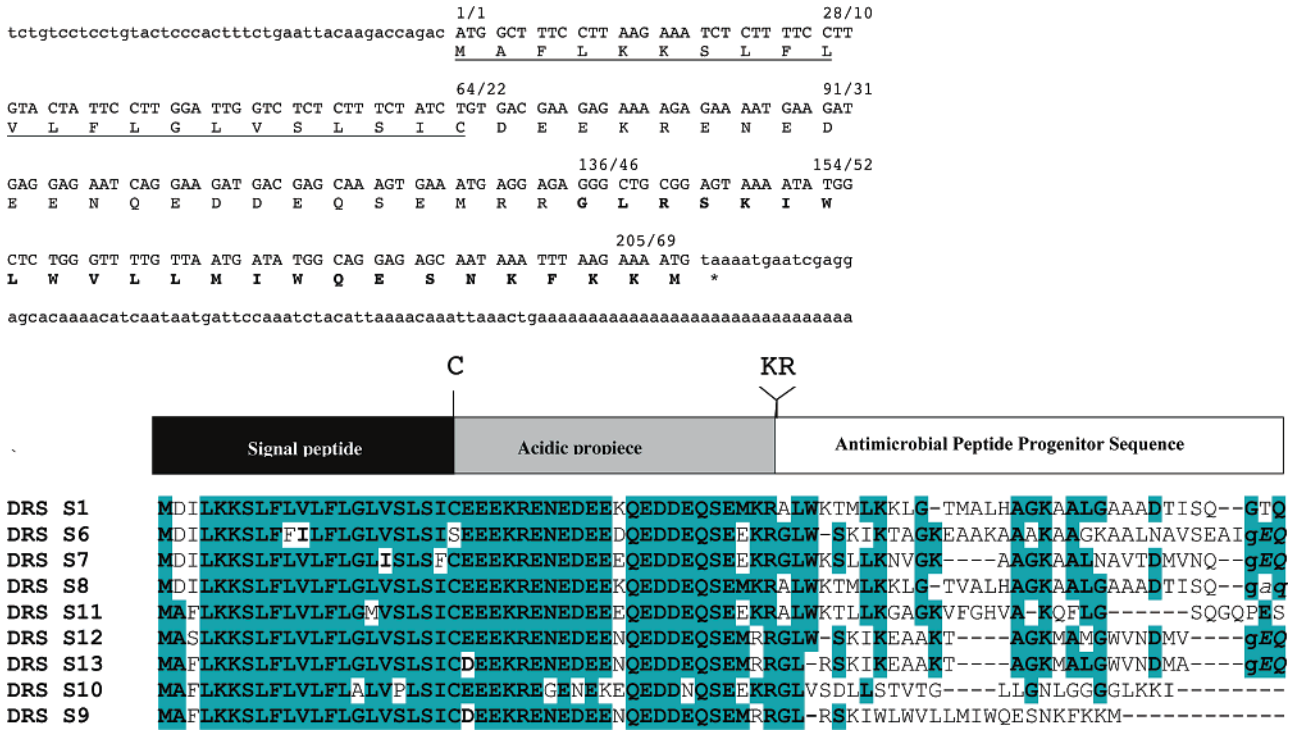

FIGURE 1: Nucleic acid and deduced amino acid sequences of cDNAs encoding dermaseptins S from the skin of *P. sauvagei*. (A) Nucleic acid and predicted amino acid sequences of the cDNA encoding dermaseptin S9. The predicted amino acid sequence is given in capital letters under the nucleotide sequence. The amino acid sequence of mature dermaseptin S9 is given in bold letters. The amino acid sequence of the signal peptide is underlined. Nucleotides and amino acids are numbered positively starting with position 1 of the open-reading frame. An asterisk indicates the stop codon. (B) Conserved preproregions and hypervariable antimicrobial domains of preprodermaseptins S. The coding region, including the signal peptide, the acidic propiece, and the antimicrobial progenitor sequence, is drawn as a rectangle. The predicted amino acid sequences (single-letter code) of preprodermaseptins S1, S6, S7, and S8 are from ref *41*, and the predicted amino acid sequences of preprodermaseptins S9, S10, S11, S12, and S13 are from this study. The predicted hydrophobic signal peptide includes the first 22 amino acid residues, while the acidic propiece (bold letters) has 23 residues. Gaps (−) have been introduced to maximize sequence similarities. Identical (shaded background) amino acid residues are highlighted. Amino acids in italic are removed during the processing of proforms to expose the extra Gly residue (lowercase letters), which serves as an amide donor for the C-terminal residue of mature peptides.

all contained a 22-residue signal peptide followed by a 23-residue acidic propiece with a pair of basic residues (Lys-Arg) at its C terminus. A single copy of a mature dermaseptin progenitor sequence was found at the extreme C terminus of the precursors flanking the acidic propiece. One of these cDNAs encoded dermaseptin S1 (*40*, *41*), while the remaining five cDNAs encoded dermaseptins whose primary structures were unknown; these were designated dermaseptins S9−S13 in accordance with the established nomenclature (Table 1) (*40*, *41*). The five novel prepropeptides all had the characteristics of dermaseptin preproforms, including a conserved signal peptide and acidic propiece whose amino acid sequences were 85−90 and 73−100% identical to those of other dermaseptin S family members (Figure 1B). This similarity extended to the 5′- and 3′-UTRs of the corresponding mRNAs (not shown). As shown previously, preprodermaseptins S6−S8 have carboxy termini that end in the tripeptide GE/AQ (*41*). Removal of the dipeptide E/AQ with carboxypeptidase or dipeptidylcarboxypeptidase during processing of these proforms exposes the extra Gly residue that serves as an amide donor for the C-terminal residue of mature dermaseptin S6−S8 (*41*). Because preprodermaseptins S12 and S13 had carboxy termini that ended in the tripeptide GEQ, the mature dermaseptins S12 and S13 are probably carboxyamidated.

Sequence Analysis of New Deduced Dermaseptins S. Although the five new dermaseptins S are genetically related, with very similar preproform signal sequences and acidic propieces, they have clearly diverged to yield three structurally distinct subfamilies. The first subfamily includes dermaseptins S11, S12, and S13, together with dermaseptins S1−S8. They are 25−34 residues long and have similar sequences (23−94% amino acid positional identity) (Table 1). They contain between 4 and 6 lysine residues, and their amino acid sequences exhibit the periodic pattern of polar and nonpolar residues characteristic of amphipathic α helices (not shown). Dermaseptin S13 does not have a Trp in position 3, as do the other members of this subfamily. Dermaseptin S10 is a prototypical member of a second subfamily with unique characteristics. The peptide is cationic, rich in glycine (28%) and leucine (28%), and contains no alanine residues. A comparison of the sequence of dermaseptin S10 with those of dermaseptins from other South American and Australian hylid frogs indicates that this peptide is structurally related to dermaseptin-related peptide (DRP)-PBN2, DRP-AA2−5, and DRP-PD3−6 from *Phyllomedusa bicolor*, *Agalychnis annae*, and *Pachymedusa dacnicolor*, respectively (*66*, *67*). Neighbor-joining and maximum parsimony studies indicated that they form a well-demarcated family of Gly-Leu-rich peptide orthologues (not shown). Previous studies have shown that these membrane-damaging peptides adopt an amphipathic α-helical conformation at membrane interfaces and are highly potent against microorganisms (*67*).

Interestingly, dermaseptin S9 is a 24-residue-long peptide that does not resemble any of the antimicrobial peptides

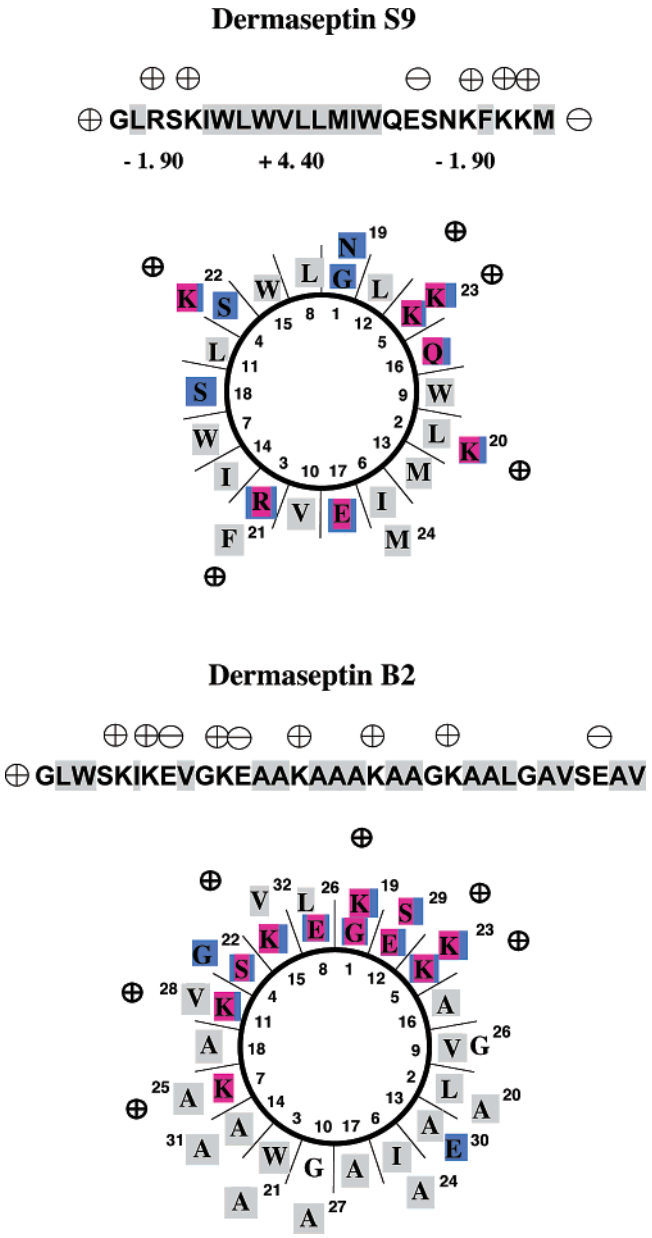

FIGURE 2: Amino acid sequences and amphipathic properties of dermaseptin S9 and dermaseptin B2. Dermaseptin B2 exhibits alternating hydrophobic and polar/charged residues along the primary structure and forms an α-helical amphipathic helix in a membrane environment, with polar and apolar amino acids on opposing surfaces along the long axis of the helix (*78*). In contrast, dermaseptin S9 has a tripartite structure comprising a highly hydrophobic core sequence (mean hydrophobicity, +4.40, determined by the Liu−Deber scale) flanked by hydrophilic and charged residue termini (mean hydrophobicity, −1.90). Dermaseptin S9 forms an α helix in a membrane environment, but polar and apolar residues are not segregated on opposing surfaces along the long axis of the helix. The hydrophobic core is nonamphipathic because it has no hydrophilic residues. Hydrophobic residues are colored in gray, and polar/charged residues are colored in blue.

identified to date (Figure 2). In sharp contrast to known helical antimicrobial peptides, dermaseptin S9 has a highly hydrophobic core sequence comprising 10 bulky aliphatic and aromatic residues (mean hydrophobicity, +4.40, determined by the Liu−Deber scale), which is flanked on either side by polar/cationic residues (mean hydrophobicity, −1.90). The hydrophobic core is regarded as nonamphipathic because there are no hydrophilic residues. This structure is reminiscent of that of synthetic peptides originally designed as transmembrane mimetic models and that spontaneously become inserted into membranes (*43*−*45*). We therefore investigated the action of dermaseptin S9 on bacterial membranes.

Table 2: Antimicrobial and Hemolytic Activities of Dermaseptin S9 and Dermaseptin B2[a]

	minimal inhibitory concentration (μM)	
microorganisms	dermaseptin S9	dermaseptin B2
Gram-negative bacteria		
Escherichia coli 363	3.1	1.5
Salmonella typhimurium	3.1	3.1
Klebsiella pneumoniae	12.5	1.5
Gram-positive bacteria		
Staphylococcus haemolyticus	12.5	6.2
Staphylococcus aureus	R	25
Bacillus megaterium	0.4	0.4
Listeria monocytogenes	0.4	nd[b]
rat erythrocytes	50% hemolysis	
	175	>500

[a] The antimicrobial activity is expressed as MIC (μM), the minimal peptide concentration required for total inhibition of cell growth in liquid medium. Results are the mean of three independent experiments each performed in duplicate. Strains were considered resistant (R) when their growth was not inhibited by peptide concentrations up to 400 μM.[b] Not determined.

Antimicrobial and Hemolytic Activities of Dermaseptin S9. The antibacterial activity of dermaseptin S9 was assayed against Gram-negative and Gram-positive bacteria (Table 2). The corresponding values for dermaseptin B2 from *P. bicolor*, a potent α-helical antimicrobial peptide from frog skin that binds to and permeates bacterial membranes (Figure 2), are shown for comparison. Although their structures are very different, dermaseptins S9 and B2 show overlapping antimicrobial spectra. They have broad-spectrum antibacterial activities, inhibiting the growth of Gram-positive and Gram-negative bacteria with minimal inhibitory concentrations in the micromolar range. The dose−response profiles showed sharp curves in which 0−100% inhibition was generated within a 1−2-fold peptide dilution (not shown). Bacteria incubated overnight with 25 μM dermaseptin S9 or dermaseptin B2 produced no colony-forming units, indicating that the peptides are bactericidal. Dermaseptin S9 has a low hemolytic activity when tested against rat erythrocytes (Table 2).

Permeabilization of the Bacterial Cytoplasmic Membrane. Disruption of the bacterial membrane by dermaseptin S9 and dermaseptin B2 was detected by incubating *E. coli* 363 with the peptide (3 μM) and measuring the hydrolysis of the chromogenic substrate, ONPG, by cytoplasmic β-galactosidase. Dermaseptin S9 permeabilized the cytoplasmic membrane of *E. coli*, as shown by the increasing release of the enzyme with increasing time, and ∼100% enzyme activity was released after 50 min of incubation (Figure 3). Thus, the bacterial membrane is one of the main targets of dermaseptin S9.

Mode of Action Studies of Dermaseptin S9. We investigated the interaction of dermaseptin S9 with model bilayers by SPR and its structure in membrane-mimetic environments by CD and two-dimensional NMR spectroscopy to analyze its membrane binding and conformational properties.

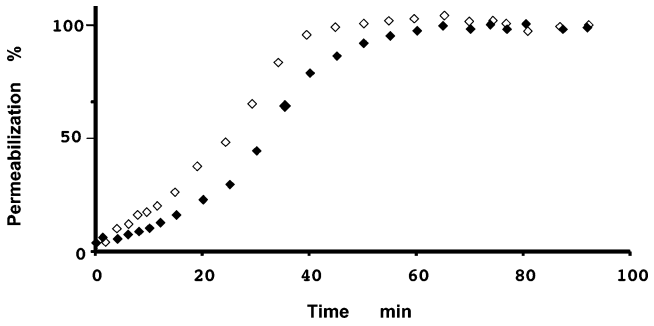

FIGURE 3: Kinetics of the cytoplasmic membrane leakage of *E. coli* after treatment with 3 μM dermaseptin S9 (◆) and dermaseptin B2 (◇). The membrane leakage was followed by measuring the hydrolysis of ONPG at 420 nm by the cytoplasmic bacterial β-galactosidase in the filtrate of *E. coli* 363 culture after incubation with the peptides (see the Materials and Methods).

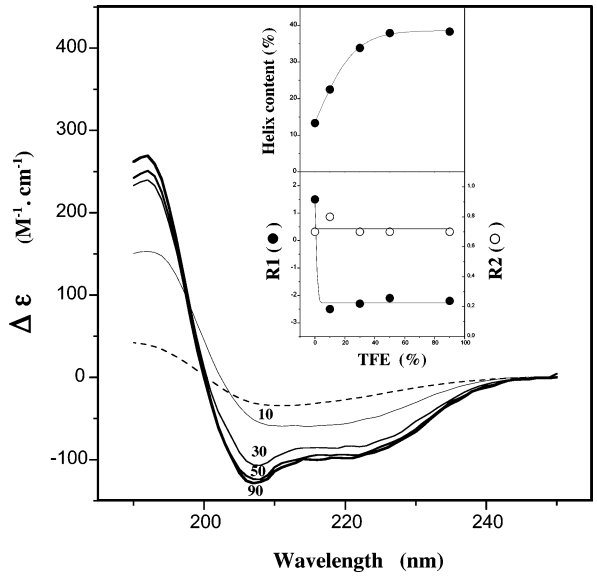

FIGURE 4: Far-UV CD spectra of dermaseptin S9 (30 mM) in aqueous solution (···) and in TFE. Numbers indicate the concentration of TFE in percentages (v/v). The insets show the helix content at increasing concentrations of TFE and R1 and R2 ratios at increasing concentrations of TFE. R1 (ratio between the intensity of the maximum between 190 and 195 nm and the intensity of the minimum between 195 and 210 nm) is ≤ -2 for highly helical peptides (>0 for a random-coil peptide), while R2 (ratio between the intensity of the minimum near 222 nm and the intensity of the minimum between 195 and 210 nm) approaches $+1$ (0 for a random-coil peptide) (*68*).

(A) Secondary Structure of Dermaseptin S9 Determined by CD Spectroscopy. Preliminary indications of the peptide secondary structure were obtained by CD measurements in water and in TFE/water mixtures (Figure 4). The CD spectrum of dermaseptin S9 (30 μM) in aqueous solution showed that the peptide has very little ordered structure in aqueous solution (··· in Figure 4). The CD spectra in TFE indicated an α-helical conformation. We analyzed the R1 and R2 ratios as a function of the TFE concentration, where R1 (ratio between the intensity of the maximum between 190 and 195 nm and the intensity of the minimum between 195 and 210 nm) is ≤ -2 for highly helical peptides (>0 for a random-coil peptide), while R2 (ratio between the intensity of the minimum near 222 nm and the intensity of the minimum between 195 and 210 nm) approaches $+1$ (0 for a random-coil peptide). The isodichroic point observed at 198 nm together with variations in the R1 and R2 ratios indicate a strong cooperative transition from random coil to α helix (*68*). The helical content increased with the TFE concentration up to 50% (v/v), corresponding to an α-helical content of 40%. Dermaseptin S9 acquired an α-helical fold also in the presence of micellar SDS (data not shown). The secondary structure predicted using the consensus prediction at the Network Protein Sequence Analysis web server indicates that the helical structure is within the central region (residues 7−22) of the peptide.

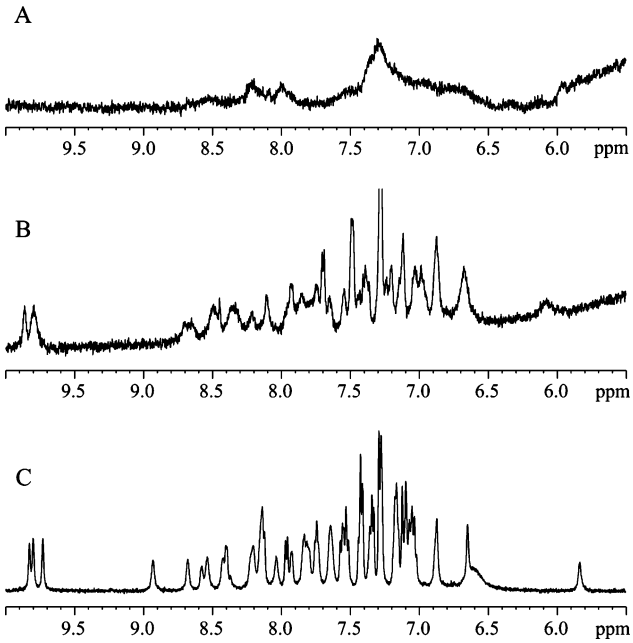

FIGURE 5: One-dimensional ^{1}H NMR spectrum of dermaseptin S9 in different environments. (A) water at 40 °C and pH 3.3, (B) 120 mM SDS at 50 °C and pH 5.4, and (C) 30% TFE at 30 °C and pH 3.3. The region shown (10−5.5 ppm) corresponds to amide and aromatic protons.

(B) NMR Spectroscopy of Dermaseptin S9: Sample Conditions. The NMR studies were conducted in different solvents to probe the conformational propensities of dermaseptin S9. The NMR spectrum of dermaseptin S9 in water (Figure 5A) shows very broad signals indicative of aggregation, despite high solubility. This aggregation state was not dependent upon variations of pH (from 3 to 7), temperature (5−45 °C), or concentration (0.1−2 mM). We also examined the effects of anionic (SDS) or zwitterionic (DPC) detergents above the micellar concentration. The addition of SDS or DPC (80−200 mM) gives rise to less-broadened signals (Figure 5B), suggesting that dermaseptin S9, although not monomeric, forms smaller aggregates in a micellar environment. In contrast, the addition of trifluoroethanol (TFE) in water reveals a unique set of sharp resonances (Figure 5C), indicating that dermaseptin S9 is likely to be monomeric in these conditions.

NMR Spectroscopy of Dermaseptin S9 in TFE. The 2D NMR spectra of dermaseptin S9 recorded in 30% TFE at 30 °C exhibited excellent chemical-shift dispersion of the amide protons and were suitable for structural investigation. The proton chemical shifts of dermaseptin S9 were assigned using the conventional strategy based on homonuclear 2D TOCSY and NOESY experiments (*69*), and the complete assignments are listed in Table S1 in the Supporting Information. Information on the secondary structure can be inferred from

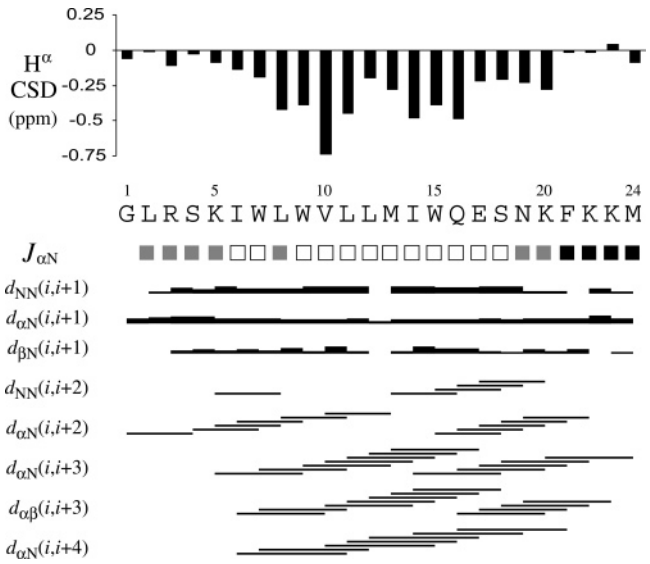

FIGURE 6: CSD of H^{α} protons, $^{3}J_{H^{N}-H^{\alpha}}$ coupling constants, and summary of sequential and medium-range NOEs observed for dermaseptin S9 in 30% TFE. The CSD values were calculated as the difference between the observed chemical shifts and random-coil chemical shifts in water (*82*, *83*). $^{3}J_{H^{N}-H^{\alpha}}$ coupling constants are represented by squares: open square, $J \leq 5.5$ Hz; gray square, $5.5 < J \leq 6.5$ Hz; filled square, $J > 6.5$ Hz. The relative intensity of NOE connectivities is indicated by horizontal bars of varying thickness.

the analysis of the CSDs of H^{α} protons, corresponding to the differences between observed chemical shifts and corresponding random-coil values determined in water. Most residues exhibit upfield shifts of H^{α} resonances that are characteristic of the helical structure (Figure 6). Using a threshold value of −0.1 ppm for the CSD, the central segment 6−20 is likely to adopt predominantly helical conformations, while the N- and C-terminal residues should be more flexible. The magnitude and pattern of interresidue nuclear Overhauser effects (NOEs) also give a qualitative indication of the secondary structure of dermaseptin S9. NOE correlations characteristic of the α-helical conformation were observed throughout the peptide chain, including strong $d\alpha N$ intraresidual correlations, strong $dNN(i, i+1)$, and medium $d\alpha N(i, i+1)$ sequential connectivities, together with numerous $d\alpha N(i, i+3)$, $d\alpha\beta(i, i+3)$, and $d\alpha N(i, i+4)$ medium-range NOE connectivities (Figure 6 and Table S2 in the Supporting Information). Furthermore, many residues exhibit $^{3}J_{H^{N}-H^{\alpha}}$ coupling constants lower than 6 Hz (Figure 6), consistent with preferential helical conformations.

NMR Spectroscopy of Dermaseptin S9 in Micellar Environments. Partial proton assignments could be obtained in SDS micelles, and nearly complete assignments were achieved in DPC micelles. Most H^{α} protons exhibit negative CSDs, indicating that helical conformations are significantly populated. However, the poor quality of the 2D NOESY spectra precluded further structural investigation.

(C) Structure of Dermaseptin S9 in TFE. The structure of dermaseptin S9 in 30% TFE was calculated by restrained molecular dynamics, using a set of 380 distance restraints (141 intraresidual, 112 sequential, and 127 medium-range NOEs) and 16 dihedral angle restraints (15 ϕ, 5 χ_1). The structures (Figure 7) exhibit low energies and few restraint violations (Table 4). The root-mean-square deviation (rmsd) of backbone atoms (N, C^{α}, and C′) is 2.0 Å. The core segment 6−21 forms a well-defined helix, with a backbone rmsd of 0.3 Å. In contrast, terminal 1−5 and 22−24 segments are more disordered, in accordance with the H^{α} CSDs. The comparison of the intensities of intraresidual and sequential dαN NOEs in segment 2−5 confirms that these residues do not explore a unique region of the Ramachandran diagram. Moreover, the presence of conformational equilibrium in the C-terminal segment is also suggested by the higher values of $^{3}J_{H^{N}-H^{\alpha}}$ coupling constants (>6.5 Hz). Therefore, the increased disorder observed in the structure family is not merely due to a lack of NMR restraints but rather reflects greater flexibility of peptide extremities. The structure is stabilized by many $i, i+3$ and $i, i+4$ van der Waals interactions between side chains (Figure 7B). The side-chain conformations correspond mainly to *gauche* + (−60°) or *trans* (180°) rotamers for the χ_1 dihedral angle. The observed NOEs of a few residues are not compatible with a unique conformation of the side chain. Trp 9, in particular, rapidly interconverts between a *gauche* + and a *trans* conformation around the χ_1 angle. The isopotential electrostatic distribution surface of the structures shows the lack of amphipathicity suggested by the amino acid sequence of the peptide (see the figure in the table of content).

(D) Binding to Lipid Bilayers as Measured by SPR. Typical sensorgrams of the binding between dermaseptin B2 and dermaseptin S9 with bilayers of DMPC are shown in parts A and B of Figure 8. The binding of the peptides increased with the peptide concentration, indicating specific interactions between the peptides and the zwitterionic surface. A comparison of the binding profiles of dermaseptin B2 and dermaseptin S9 showed that the peptides differ in their binding affinity (as revealed by the binding levels) and kinetics, with significant differences in the association and dissociation rates for the lipid surface. The initial association and dissociation of dermaseptin B2 with the zwitterionic membrane were very rapid and then slowed. The binding of dermaseptin S9 proceeded with slower kinetics, and most of the adsorbed peptide remained bound to the lipid or inserted into the bilayer. The sensorgram curves were fitted to a two-state model using BIA evaluation 3.0 software

$$P + L \overset{K_{A_1}}{\longleftrightarrow} PL \overset{K_{A_2}}{\longleftrightarrow} PL^{*}$$

K_{A_1}, the first stage association affinity constant indicates the adsorption of the peptide to the membrane surface (primary binding), whereas K_{A_2} is unitless and reflects the tendency of the peptides to become inserted into or to assemble on the membrane and subsequently move from the surface to become inserted (*67*, *70*, *72*). The association (k_{a_1}, k_{a_2}) and dissociation (k_{d_1}, k_{d_2}) rate constants along with the individual affinity constants (K_{A_1}, K_{A_2}) of each stage of the interaction are listed in Table 3. The calculated overall equilibrium constants, $K_A = K_{A_1} \times K_{A_2}$, for the binding of the peptides to the zwitterionic membrane demonstrated that the affinity of dermaseptin B2 is 20 times greater than that of dermaseptin S9. This is because dermaseptin B2 binds 5 times more efficiently than dermaseptin S9 in the first step (K_{A_1}) and inserts 4-fold better in the second step (K_{A_2}).

The sensorgrams for dermaseptin B2 and dermaseptin S9, interacting with anionic DMPG membranes, and the monitoring of the DMPG bilayer formation and peptide binding on the L1 sensor chip surface are compared in parts C and

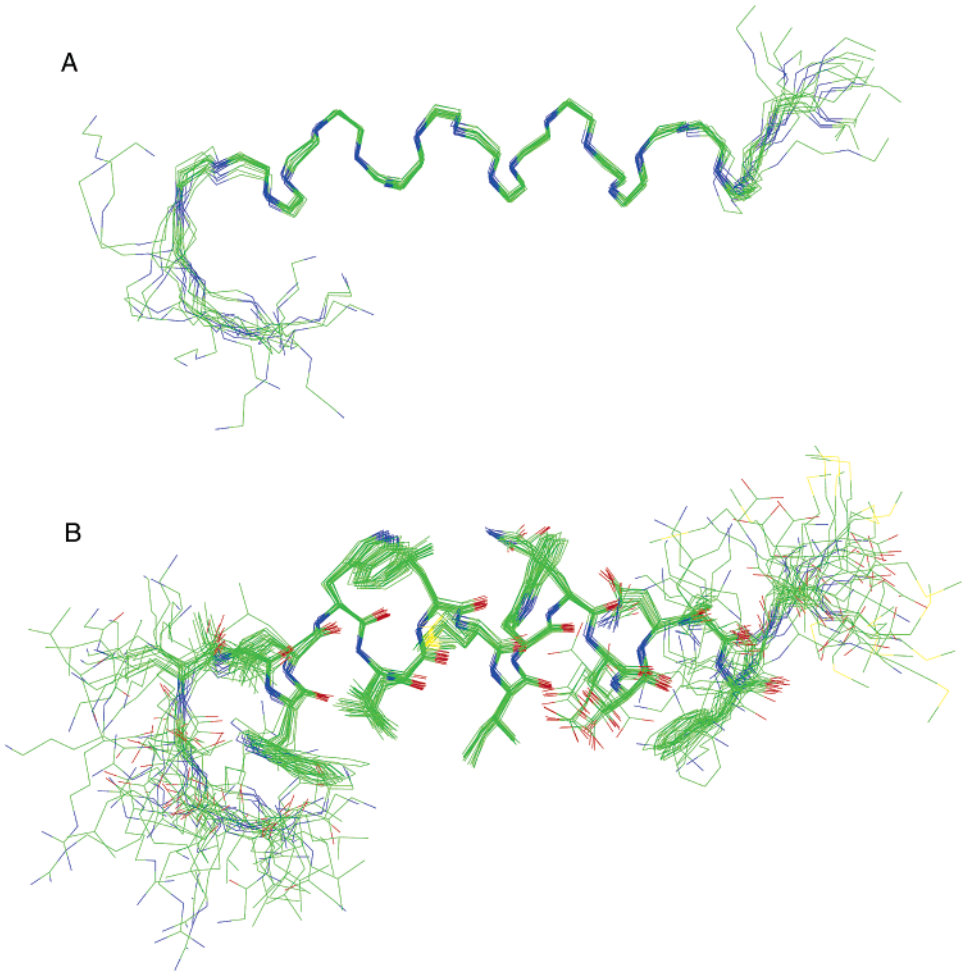

FIGURE 7: Three-dimensional solution structure of dermaseptin S9 in 30% TFE. Structures were superimposed by best fitting of backbone N, C^{α}, and C′ atoms from residues 6 to 21. (A) Backbone atoms. (B) Backbone and side chain heavy atoms.

D of Figure 8, and it is immediately apparent that the peptides behave differently. The equilibrium binding level of dermaseptin B2 to DMPG reached ~1000 RU for the bulk peptide concentration below 10 μM (Figure 8C). This approximates the formation of a monolayer of peptide on the surface. Most of this layer is not desorbed upon washing. At a bulk peptide concentration >10 μM, dermaseptin B2 continued to accumulate on the anionic surface during the entire injection phase without reaching an equilibrium level. This may reflect the formation of multiple layers of peptide on the surface, i.e., self-assembly of surface-adsorbed monomers (*70*). A significant portion of these peptide layers was removed by the buffer flow. Table 3 summarizes the obtained kinetic rate constants and the affinity constants for the interaction of dermaseptin B2 with DMPG bilayers as determined using the two-state model. Note that this model assumes that the reactants are monomers. Because surface-adsorbed monomers of dermaseptin B2 aggregate to form multiple layers of membrane-bound peptide when a critical peptide concentration is reached, values in Table 3 should be considered as indicative only. Dermaseptin B2 interacts preferentially with anionic lipids ~7-fold stronger than with zwitterionic lipids. This difference in binding is mainly due to the second binding step, i.e., the tendency of the peptide to assemble on the membrane surface and subsequently move from the surface to become inserted.

SPR experiments performed with dermaseptin S9 under the same conditions demonstrated a quite different behavior. As shown in Figure 8D, the baseline following regeneration of the L1 sensor chip surface by removal of the DMPG bilayer by injection of octyl-glucoside was good with dermaseptin B2, with a linear drift over the various cycles not exceeding 2 RU per cycle. The surface was then reused many times. In contrast, full regeneration of the sensor chip was not possible with dermaseptin S9, even after a single cycle of binding (Figure 8D). An explanation may be that dermaseptin S9, probably because it inserts deep into the inner leaflet, interacts with the alkyl chains covalently linked to the dextran-coated gold surface of the sensor chip, with a significant fraction of the peptide remaining irreversibly bound. As a result, global data fitting allowing kinetic parameters to be derived simultaneously from several sensorgrams was not accessible. Thus, only an estimate of the kinetic and equilibrium parameters of dermaseptin S9 was obtained by using a local fit model on two sensorgrams. Dermaseptin S9 interacts preferentially with anionic lipids ~100-fold stronger than that with zwitterionic lipids and 7 times better than dermaseptin B2. In both cases, this is the result of the second step and not the first step.

DISCUSSION

Preprodermaseptins are polypeptide precursors found in hylid frog skin. The members of this rapidly expanding

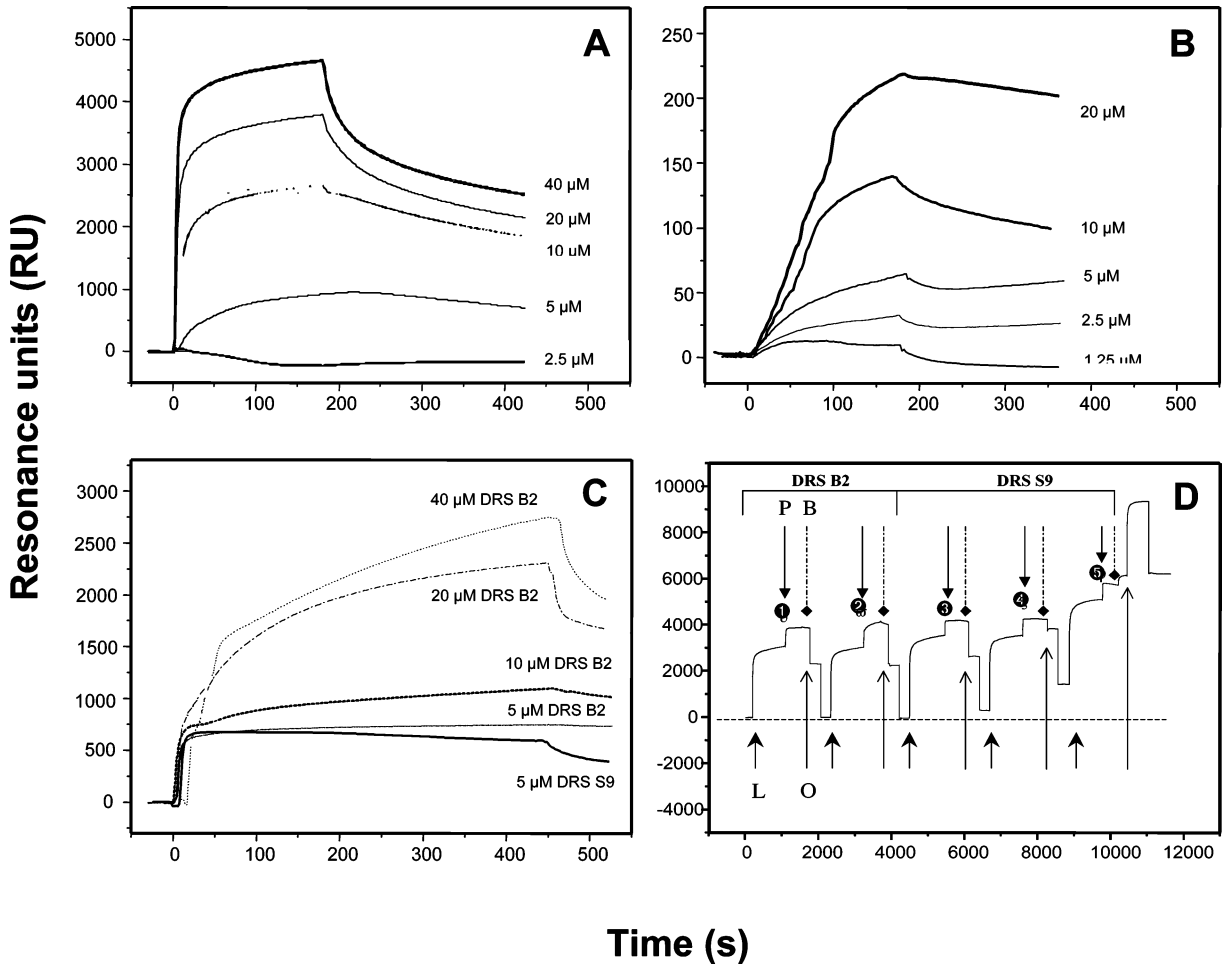

FIGURE 8: (A) SPR sensorgrams of the binding between various concentrations of dermaseptin B2 and the zwitterionic bilayer DMPC at pH 7. Injections were made at time = 0 min, and PBS was added to initiate dissociation at 180 s. (B) SPR sensorgrams of the binding between various concentrations of dermaseptin S9 and the zwitterionic bilayer DMPC at pH 7. (C) Sensorgrams of the binding between dermaseptin B2 and dermaseptin S9 and the anionic bilayer DMPG. (D) Monitoring the lipid bilayer formation on the L1 sensor chip surface and peptide binding onto the DMPG bilayer. L, LUV deposition; P, peptide injections; circled 1, 5 μM dermaseptin (DRS) B2; circled 2, 10 μM DRS B2; circled 3, 1.25 μM DRS S9; circled 4, 2.5 μM DRS S9; circled 5, 5 μM DRS S9; B, running buffer (PBS); O, regeneration step by *N*-octyl-β-D-glucopyranoside.

Table 3: Equilibrium Affinity Constants and Association [k_{a_1} (M^{-1} s^{-1}), k_{a_2} (s^{-1})] and Dissociation [k_{d_1} (s^{-1}), k_{d_2} (s^{-1})] Rate Constants of Dermaseptin B2 and Dermaseptin S9 with DMPC and DMPG Bilayers Determined by Numerical Integration Using the Two-State Model[a]

	dermaseptin B2		dermaseptin S9	
	DMPC	DMPG	DMPC	DMPG
k_{a_1}	8.0×10^3	2.3×10^4	2.8×10^2	3.0×10^4
k_{d_1}	5.5×10^{-3}	9.0×10^{-3}	9.4×10^{-4}	1.3×10^{-2}
k_{a_2}	1.1×10^{-2}	5.2×10^{-3}	1.2×10^{-5}	1.2×10^{-3}
k_{d_2}	2.1×10^{-3}	2.5×10^{-4}	1.0×10^{-5}	7.8×10^{-6}
K_{A_1}	1.4×10^6	2.6×10^6	3.0×10^5	2.3×10^6
K_{A_2}	5.2	20.8	1.2	154
K_A	7.6×10^6	5.3×10^7	3.6×10^5	3.5×10^8

[a] The affinity constants K_{A_1} (M^{-1}) and K_{A_2} (unitless) are for the first ($K_{A_1} = k_{a_1}/k_{d_1}$) and second ($K_{A_2} = k_{a_2}/k_{d_2}$) steps, respectively, and the affinity constant (K_A) determined as (k_{a_1}/k_{d_1}) × (k_{a_2}/k_{d_2}) is for the complete binding process.

family all have remarkably well-conserved preproregions and markedly diverse C-terminal domains that give rise to cationic antimicrobial peptides with different lengths, sequences, target specificities, and efficiencies. Different hylid frogs have sets of homologous but different peptides that have diversified in a species-specific manner. The mature antimicrobial peptides have all been given individual names and grouped into distinct families on the basis of their origins and/or structural characteristics. They include the dermaseptins B, phylloxins, and dermatoxins from *P. bicolor*, *P. oreades*, and *P. distincta* (*40*, *46*, *47*, *49*, *73*), several Gly-Leu-rich peptides from *P. bicolor*, *A. annae*, and *P. dacnicolor* (*66*, *67*), and caerins and aureins that are produced by hylid frogs of the genus *Litoria* (*39*, *74*). The impressive diversity of these peptides is due to multiple duplications of a common ancestral gene before and during radiation of these species and within individual species and accelerated mutations of the mature peptide domain and subsequent actions of diversifying (positive) selection (*14*, *39*, *75*). While they differ widely in amino acid sequence, net positive charge, and length, all of these peptides are amphipathic with alternating hydrophobic and polar residues along the primary structure and form α helices in a membrane environment (Figure 2) (*76*−*80*). According to the Shai−Matsuzaki−Huang model, the peptides first bind to the membrane surface and then adopt a helical amphipathic structure that promotes their insertion into the membrane, which breaks up the lipid chains, causing transient pore formation and the eventual

Table 4: Structural Statistics for the Family of 20 Structures of Dermaseptin S9 in TFE

rms deviation of residual constraint violations		
distance constraints (Å)	0.022 ± 0.001	
dihedral constraints (deg)	1.8 ± 0.6	
rms deviation from idealized covalent geometry[a]		
bond lengths (pm)	0.97 ± 0.01	
bond angles (deg)	1.78 ± 0.05	
improper torsion angles (deg)	1.62 ± 0.25	
nonbond energy terms[b]		
van der Waals energy (kcal mol^{-1})[b]	-64.9 ± 4.6	
electrostatic energy (kcal mol^{-1})[b]	-11.6 ± 4.6	
Ramachandran diagram (% residues)[c]		
most favored regions	80.7	
additional allowed regions	15.9	
generous allowed regions	2.3	
disallowed regions	1.1	
mean pairwise rmsd (Å)		
	backbone atoms (N, C$^{\alpha}$, C′)	all heavy atoms
all residues (1−24)	2.03	2.88
residues 6−21	0.33	0.95

[a] Idealized covalent geometry defined by the CHARMM22 force field implemented within XPLOR-NIH. [b] Nonbond energy terms were calculated with a 12 Å cutoff; the electrostatic term was added in the final stage of minimization and was calculated with a distance-dependent dielectric $\epsilon = 4r$. [c] Ramachandran diagram regions as defined in PROCHECK-NMR.

collapse of the membrane at a critical peptide concentration (*20*−*23*).

We have sequenced new preprodermaseptin mRNAs from *P. sauvagei* to examine in more detail the structure diversity among dermaseptin S paralogues. The most unexpected result was the discovery of the cationic hydrophobic peptide, dermaseptin S9, whose structure is very different from other naturally occurring antimicrobial peptides known to date. It resembles the synthetic peptides designed as transmembrane segment mimics with a highly hydrophobic, nonamphipathic central core flanked by positively charged termini (*43*−*45*). These α-helical peptides, of the prototypical sequence KK-$(A)_3X(A)_5X(A)_2W(A)_2X(A)_3$KKKamide, become spontaneously inserted into membranes and have antibacterial activity in the micromolar range when the average hydrophobicity of their core segment is above 0.4 (i.e., X is either Y, C, V, M, I, L, W, or F) based on the Liu−Deber hydrophobicity scale. The antimicrobial activity increases with the hydrophobicity of the 19-residue core segment, and even truncated highly hydrophobic peptides of 15 or 11 core residues retain their activity. Dermaseptin S9 has a 10-residue core segment composed of bulky aliphatic and aromatic residues, with an overall segmental hydrophobicity of +4.40. The core also contains three Trp residues that are especially favored at the interface of phospholipid membranes. Although its hydrophobic core is too short to span a typical bilayer, the antimicrobial activity of dermaseptin S9 against Gram-positive and Gram-negative bacteria is comparable to that of dermaseptin B2, a 33-residue amphipathic helical peptide, which is one of the most potent peptides of the dermaseptin family. The SPR analysis showed that dermaseptin S9 binds to model bilayers, and permeabilization assays revealed that this peptide permeates bacterial membranes at a micromolar concentration and is also hemolytic at higher concentrations. CD and NMR spectroscopy combined with molecular dynamics calculations indicated that this cationic hydrophobic peptide has a high helical propensity in the presence of TFE. The central segment 6−21 adopts a well-defined helix, while the N- and C-terminal extremities are more disordered, which fits well with the results of secondary-structure prediction algorithms. NMR spectroscopy showed that dermaseptin S9 is aggregated in water at millimolar concentrations and partially aggregated in micellar solutions. The aggregation in solution is probably driven by hydrophobic interactions involving the inner apolar 6−15 segment. The peptide was not amenable to complete structure determination in these micellar environments because of the poor quality and the low signal-to-noise ratio of 2D NMR spectra. However, a preliminary analysis based on H^{α} chemical shifts suggests the presence of helical structures in these membrane-mimicking environments. The aggregative properties of dermaseptin S9 are not unique among the antimicrobial peptides because dermaseptin S4 was previously found to be highly aggregated in solution, even in the presence of TFE (*30*). We have also shown that dermaseptin B2 oligomerized in SDS micelles at a high peptide/detergent ratio, as suggested by the high complexity of its NMR spectra (*78*). Therefore, this aggregation property may be an important feature in the membrane disruption mechanism of the antimicrobial peptides.

The results of the SPR study revealed that dermaseptin S9 shows a higher binding affinity to membranes containing anionic phospholipids than zwitterionic phospholipids. This indicates that electrostatic interactions are important for the selectivity of the cationic peptide for negatively charged membranes. Interestingly, despite much weaker hemolytic activity, dermaseptin B2 binds to zwitterionic membranes more efficiently than dermaseptin S9, demonstrating that membrane binding is not sufficient to promote cytolytic activity. The results also revealed a major difference between the mode of action of dermaseptin S9 and dermaseptin B2 in DMPG membranes. Linear α-helical amphipathic peptides, such as dermaseptin B2, bind to the surface of phospholipid membranes but do not become deeply inserted into the acyl core because of the snorkeling of the regularly spaced lysine side chains of the peptide that grip it to the membrane surface. In contrast, the hydrophobic core region of dermaseptin S9 is not constrained by amphipathicity to remain at the membrane surface and may penetrate deeply into the bilayer, thereby disorganizing the lipid packing. As shown in Table 3, dermaseptin B2 and dermaseptin S9 bind with similar affinities to anionic membranes, but dermaseptin S9 inserts ∼8-fold better into the membrane interior. However, dermaseptin S9 has three tryptophan residues in the hydrophobic core, which would prefer the bilayer interface rather than the hydrophobic interior. Hence, more definitive evidence would be neeeded to assess how dermaseptin S9 binds to and permeates bacterial membranes.

The preprodermaseptin gene family encodes at least two structurally different groups of helical cationic antimicrobial peptides; the amphipathic peptides such as dermaseptins B and dermaseptins S1−S8 and hydrophobic peptides with cationic termini like dermaseptin S9. The peptides of both groups bind to and permeate membrane bilayers, despite their very different structural and biochemical properties. The presence of antimicrobial peptides with such different structures and spectra of action may represent the successful

evolution of multidrug defense by providing frogs with maximum protection against infectious microbes and minimizing the chance of microorganisms developing resistance to individual peptides.

ACKNOWLEDGMENT

Dr. Owen Parkes is acknowledged for assistance in preparing the manuscript.

SUPPORTING INFORMATION AVAILABLE

Table S1, proton assignment of dermaseptin S9; Table S2, list of the NOE restraints. This material is available free of charge via the Internet at http://pubs.acs.org.

REFERENCES

1. Brogden, K. A., Ackermann, M., McCray, P. B., Jr., and Tack, B. F. (2003) Antimicrobial peptides in animals and their role in host defences, *Int. J. Antimicrob. Agents 22*, 465−478.
2. Mor, A. (2003) Gene-encoded antimicrobial peptides. Introduction, *Peptides 24*, 1815−1821.
3. Zasloff, M. (2002) Antimicrobial peptides of multicellular organisms, *Nature 415*, 389−395.
4. Ganz, T. (2001) Antimicrobial proteins and peptides in host defense, *Semin. Respir. Infect. 16*, 4−10.
5. Gennaro, R., and Zanetti, M. (2000) Structural features and biological activities of the cathelicidin-derived antimicrobial peptides, *Biopolymers 55*, 31−49.
6. Hancock, R. E., and Scott, M. G. (2000) The role of antimicrobial peptides in animal defenses, *Proc. Nat. Acad. Sci. U.S.A. 97*, 8856−8861.
7. Kourie, J. I., and Shorthouse, A. A. (2000) Properties of cytotoxic peptide-formed ion channels, *Am. J. Physiol. Cell Physiol. 278*, C1063−C1087.
8. Bulet, P., Hetru, C., Dimarcq, J. L., and Hoffmann, D. (1999) Antimicrobial peptides in insects; structure and function, *Dev. Comp. Immunol. 23*, 329−344.
9. Epand, R. M., and Vogel, H. J. (1999) Diversity of antimicrobial peptides and their mechanisms of action, *Biochim. Biophys. Acta 1462*, 11−28.
10. Andreu, D., and Rivas, L. (1998) Animal antimicrobial peptides: An overview, *Biopolymers 47*, 415−433.
11. Simmaco, M., Mignogna, G., and Barra, D. (1998) Antimicrobial peptides from amphibian skin: What do they tell us? *Biopolymers 47*, 435−450.
12. Rinaldi, A. C. (2002) Antimicrobial peptides from amphibian skin: An expanding scnenario, *Curr. Opin. Chem. Biol. 6*, 799−804.
13. Nascimento, A. C., Fontes, W., Sebben, A., and Castro, M. S. (2003) Antimicrobial peptides from anurans skin secretions, *Protein Pept. Lett. 10*, 227−238.
14. Nicolas, P., Vanhoye, D., and Amiche, M. (2003) Molecular strategies in biological evolution of antimicrobial peptides, *Peptides 24*, 1669−1680.
15. Apponyi, M. A., Pukala, T. L., Brinkworth, C. S., Maselli, V. M., Bowie, J. H., Tyler, M. J., Booker, G. W., Wallace, J. C., Carver, J. A., Separovic, F., Doyle, J., and Llewellyn, L. E. (2004) Host-defense peptides of Australian anurans: Structure, mechanism of action, and evolutionary significance, *Peptides 25*, 1035−1054.
16. Conlon, J. M., Kolodziejek, J., and Nowotny, N. (2004) Antimicrobial peptides from ranid frogs: Taxonomic and phylogenetic markers and a potential source of new therapeutic agents, *Biochim. Biophys. Acta 1696*, 1−14.
17. Tossi, A. A database with more than 400 entries, http://www.bbcm.univ.trieste.it/~tossi/ search.html.
18. Segrest, J. P., De Loof, H., Dohlman, J. G., Brouillette, C. G., and Anantharamaiah, G. M. (1990) Amphipathic helix motif: Classes and properties, *Proteins 8*, 103−117.
19. Ehrenstein, G., and Lecar, H. (1977) Electrically gated ionic channels in lipid bilayers, *Q. Rev. Biophys. 10*, 1−34.
20. Matsuzaki, K. (1998) Magainins as paradigm for the mode of action of pore forming polypeptides, *Biochim. Biophys. Acta 1376*, 391−400.
21. Hancock, R. E. (1999) Peptide antibiotics, *Antimicrob. Agents Chemother. 93*, 1317−1323.
22. Huang, H. W. (2000) Action of antimicrobial peptides: 2-State model, *Biochemistry 39*, 8347−8352.
23. Shai, Y. (2002) Mode of action of membrane active antimicrobial peptides, *Biopolymers 66*, 236−248.
24. Zelezetsky, I., Pacor, S., Pag, U., Papo, N., Shai, Y., Sahl, G., and Tossi, A. (2005) Controlled alteration of the shape and conformational stability of α helical cell-lytic peptides: Effect on mode of action and cell specificity, *Biochem. J. 390*, 177−188.
25. Park, I. Y., Cho, J. H., Kim, K. S., Kim, Y. B., and Kim, S. C. (2004) Helix stability confers salt resistance upon helical antimicrobial peptides, *J. Biol. Chem. 279*, 13896−13901.
26. Dennison, S. R., Harris, F., and Phoenix, D. A. (2003) Factors determining the efficacy of α helical antimicrobial peptides, *Protein Pept. Lett. 10*, 497−502.
27. Papo, N., and Shai, Y. (2003) Can we predict biological activity of antimicrobial peptides from their interactions with model phospholipid membranes? *Peptides 24*, 1693−1703.
28. Powers, J. P., and Hancock, R. E. (2003) The relationship between peptide structure and antibacterial activity, *Peptides 24*, 1681−1691.
29. Dathe, M., Meyer, J., Beyermann, M., Maul, B., Hoischen, C., and Bienert, M. (2002) General aspects of peptide selectivity towards lipid bilayers and cell membranes studied by variation of the structure parameters of amphipathic helical model peptides, *Biochim. Biophys. Acta 1558*, 171−186.
30. Kustanovich, I., Shalev, D. E., Mikhlin, M., Gaidukov, L., and Mor, A. (2002) Structural requirements for potent versus selective cytotoxicity for antimicrobial dermaseptin S4 derivatives, *J. Biol. Chem. 277*, 16941−16951.
31. Tochi, T., Epand, R. F., Epand, R. M., and Matsuzaki, K. (2002) Position-dependent hydrophobicity of the antimicrobial magainin peptide affects the mode of peptide−lipid interaction and selectivity, *Biochemistry 41*, 10723−10731.
32. Giangaspero, A., Sandri, L., and Tossi, A. (2001) Amphipathic α helical peptides, *Eur. J. Biochem. 268*, 5589−5600.
33. Bechinger, B. (1999) The structure, dynamics, and orientation of antimicrobial peptides in membranes by solid-phase NMR spectroscopy, *Biochim. Biophys. Acta 1462*, 157−183.
34. Blondelle, S. E., Lohner, K., and Aguilar, M. (1999) Lipid-induced conformation and lipid binding properties of cytolytic and antimicrobial peptides: Determination and biological specificity, *Biochim. Biophys. Acta 1462*, 89−108.
35. Matsuzaki, K. (1999) Why and how are peptide−lipid interactions utilized for self-defense? Magainins and tachyplesins as archetypes, *Biochim. Biophys. Acta 1462*, 1−10.
36. Sitaram, N., and Nagaraj, R. (1999) Interaction of antimicrobial peptides with biological and model membranes: Structural and charge requirements for activity, *Biochim. Biophys. Acta 1462*, 29−54.
37. Shai, Y. (1999) Mechanism of the binding, insertion, and destabilization of phospholipid bilayer membranes by α-helical antimicrobial and cell non-selective membrane-lytic peptides, *Biochim. Biophys. Acta 1462*, 55−70.
38. Papo, N., Oren, Z., Pag, U., Sahl, H. G., and Shai, Y. (2002) The consequence of sequence alteration of an amphipathic α-helical antimicrobial peptide and its diastereomers, *J. Biol. Chem. 277*, 33913−33921.
39. Vanhoye, D., Bruston, F., Nicolas, P., and Amiche M. (2003) Antimicrobial peptides from hylid and ranin frogs originated from a 150-mya ancestral precursor with a conserved signal peptide but a hypermutable antimicrobial domain, *Eur. J. Biochem. 270*, 2068−2081.
40. Mor, A., Hani, K., and Nicolas, P. (1994) The vertebrate peptide antibiotics dermaseptins have overlapping structural features but target specific microorganisms, *J. Biol. Chem. 269*, 31635−31641.
41. Chen, T., Tang., L., and Shaw, C. (2003) Identification of three novel *Phyllomedusa sauvagei* dermaseptins by cloning from a skin secretion-derived cDNA library, *Regul. Peptides 116*, 139−146.
42. Amiche, M., Seon, A. A., Pierre, T. N., and Nicolas, P. (1999) The dermaseptin precursors: A protein family with a common preproregion and a variable C-terminal antimicrobial domain, *FEBS Lett. 456*, 352−356.
43. Liu, L. P., and Deber, C. M. (1998) Guidelines for membrane protein engineering derived from *de novo* designed model peptides, *Biopolymers 47*, 41−62.

44. Stark, M., Liu, L. P., and Deber, C. M. (2002) Cationic hydrophobic peptides with antimicrobial activity, *Antimicrob. Agents Chemother. 46*, 3585−3590.
45. Chan, C., Burrows, L. L., and Deber, C. M. (2004) Helix induction in antimicrobial peptides by alginate in biofilms, *J. Biol. Chem. 279*, 38749−38754.
46. Charpentier, S., Amiche, M., Mester, Y., Vouille, V., Le Caer, J. P., Nicolas, P., and Delfour, A. (1998) Structure, synthesis, and molecular cloning of dermaseptins B, a family of skin peptide antibiotics, *J. Biol. Chem. 273*, 14690−14696.
47. Pierre, T. N., Seon, A. A., Amiche, M., and Nicolas, P. (2000) Phylloxin, a novel peptide antibiotic of the dermaseptin family of antimicrobial/opioid peptide precursors, *Eur. J. Biochem. 267*, 370−378.
48. Sambrook, J., Fritsch, E. F., and Maniatis, T. (1989) *Molecular Cloning. A Laboratory Manual*, 2nd ed., Cold Spring Harbor Laboratory, Cold Spring Harbor, NY.
49. Amiche, M., Séon, A., Wroblewski, H., and Nicolas, P. (2000) Isolation of dermatoxin from frog skin, an antibacterial peptide encoded by a novel member of the dermaseptin genes family, *Eur. J. Biochem. 267*, 4583−4592.
50. Zhong, L., and Johnson, W. C., Jr. (1992) Environment affects amino acid preference for secondary structure, *Proc. Natl. Acad. Sci. U.S.A. 89*, 4462−4465.
51. Matsuzaki, K., Murase, O., Sugishita, K., Yoneyama, S., Akada, K., Ueha, M., Nakamura, A., and Kobayashi, S. (2000) Optical characterization of liposomes by right angle light scattering and turbidity measurements, *Biochim. Biophys. Acta Biomembr. 1467*, 219−226.
52. Sklenar, V., Piotto, M., Leppik, R., and Saudek, V. (1993) Gradient-tailored water suppression for proton-nitrogen-15 HSQC experiments optimized to retain full sensitivity, *J. Magn. Reson. A 102*, 241−245.
53. Davis, D. G., and Bax, A. (1985) Assignment of complex proton NMR spectra via two-dimensional homonuclear Hartmann−Hahn spectroscopy, *J. Am. Chem. Soc. 107*, 2820−2821.
54. Griesinger, C., Otting, G., Wüthrich, K., and Ernst, R. R. (1988) Clean TOCSY for proton spin system identification in macromolecules, *J. Am. Chem. Soc. 110*, 7870−7872.
55. Kumar, A., Ernst, R. R., and Wüthrich, K. (1980) A two-dimensional nuclear Overhauser enhancement (2D NOE) experiment for the elucidation of complete proton−proton cross-relaxation networks in biological macromolecules, *Biochem. Biophys. Res. Commun. 95*, 1−6.
56. Lippens, G., Dhalluin, C., and Wieruszeski, J. M. (1995) Use of a water flip-back pulse in the homonuclear NOESY experiment, *J. Biomol. NMR 5*, 327−331.
57. Rance, M., Sørensen, O. W., Bodenhausen, G., Wagner, G., Ernst, R. R., and Wüthrich, K. (1983) Improved spectral resolution in COSY proton NMR spectra of proteins via double quantum filtering, *Biochem. Biophys. Res. Commun. 117*, 479−485.
58. Schleucher, J., Schwendinger, M., Sattler, M., Schmidt, P., Schedletzky, O., Glaser, S. J., Sorensen, O. W., and Griesinger, C. (1994) A general enhancement scheme in heteronuclear multidimensional NMR employing pulsed field gradients, *J. Biomol. NMR 4*, 301−306.
59. Bartels, C., Xia, T. H., Billeter, M., Güntert, P., and Wüthrich, K. (1995) The program XEASY for computer-supported NMR spectral analysis of biological macromolecules, *J. Biomol. NMR 6*, 1−10.
60. Szyperski, T., Güntert, P., Otting, G., and Wüthrich, K. (1992) Determination of scalar coupling constants by inverse Fourier transformation of in-phase multiplets, *J. Magn. Reson. 99*, 552−560.
61. Güntert, P., Mumenthaler, C., and Wüthrich, K. (1997) Torsion angle dynamics for NMR structure calculation with the new program DYANA, *J. Mol. Biol. 273*, 283−298.
62. Wüthrich, K., Billeter, M., and Braun, W. (1983) Pseudo-structures for the 20 common amino acids for use in studies of protein conformations by measurements of intramolecular proton−proton distance constraints with nuclear magnetic resonance, *J. Mol. Biol. 169*, 949−961.
63. Ludvigsen, S., and Poulsen, F. M. (1992) Positive φ-angles in proteins by nuclear magnetic resonance spectroscopy, *J. Biomol. NMR 2*, 227−233.
64. Schwieters, C. D., Kuszewski, J. J., Tjandra, N., and Clore, M. G. (2003) The Xplor-NIH NMR molecular structure determination package, *J. Magn. Reson. 160*, 65−73.
65. Laskowski, R. A., Rullmannn, J. A., MacArthur, M. W., Kaptein, R., and Thornton, J. M. (1996) AQUA and PROCHECK-NMR: Programs for checking the quality of protein structures solved by NMR, *J. Biomol. NMR 8*, 477−486.
66. Wechselberger, C. (1998) Cloning of cDNAs encoding new peptides of the dermaseptin family, *Biochim. Biophys. Acta 1388*, 279−283.
67. Vanhoye, D., Bruston, F., El Amri, S., Ladram, A., Amiche, M., and Nicolas, P. (2004) Membrane association, electrostatic sequestration, and cytotoxicity of Gly-Leu-rich peptide orthologs with differing functions, *Biochemistry 43*, 8391−8409.
68. Bruch, M. D., Dhingra, M. M., and Gierasch, L. M. (1991) Side chain−backbone hydrogen bonding contributes to helix stability in peptides derived from an α-helical region of carboxypeptidase A, *Proteins 10*, 130−139.
69. Wüthrich, K. (1986) *NMR of Proteins and Nucleic Acids*, Wiley, New York.
70. Gaidukov, L., Fish, A., and Mor, A. (2003) Analysis of membrane-binding properties of dermaseptin analogues: Relationships between binding and cytotoxicity, *Biochemistry 42*, 12866−12874.
71. Chia, C. S. B., Torres, J., Cooper, M. A., Arkin, I. T., and Bowie, J. H. (2002) The orientation of the antibiotic peptide maculatin 1.1 in DMPG and DMPC lipid bilayers. Support for a pore-forming mechanism, *FEBS Lett. 512*, 47−51.
72. Papo, N., and Shai, Y. (2003) Exploring peptide membrane interaction using surface plasmon resonance: Differentiation between pore formation versus membrane disruption by lytic peptides, *Biochemistry 42*, 458−466.
73. Brand, G. D., Leite, J. R., Silva, L. P., Albuquerque, S., Prates, M. V., Azevedo, R. B., Carregaro, V., Da Silva, J. S., Sa, V. C., Brandao, R. A., and Bloch, C., Jr. (2002) Dermaseptins from *Phyllomedusa oreades* and *Phyllomedusa distincta*. Anti-*Trypanosoma cruzi* activity without cytotoxicity to mammalian cells, *J. Biol. Chem. 277*, 49332−49340.
74. Chen, T., Scott, C., Tang, L., Zhou, M., and Shaw, C. (2005) The structural organization of aurein precursor cDNAs from the skin secretion of the Australian green and golden bell frog, *Litoria aurea*, *Regul. Pept. 128*, 75−83.
75. Duda, T. F., Vanhoye, D., and Nicolas, P. (2002) Roles of diversifying selection and coordinated evolution in the evolution of amphibian antimicrobial peptides, *Mol. Biol. Evol. 19*, 858−864.
76. Feder, R., Dagan, A., and Mor, A. (2000) Structure−activity relationship study of antimicrobial dermaseptin S4 showing the consequences of peptide oligomerization on selective cytotoxicity, *J. Biol. Chem. 275*, 4230−4328.
77. Shalev, D. E., Mor, A., and Kustanovich, I. (2002) Structural consequences of carboxyamidation of dermaseptin S3, *Biochemistry 41*, 7312−7317.
78. Lequin, O., Bruston, F., Convert, O., Chassaing, G., and Nicolas, P. (2003) Helical structure of dermaseptin B2 in a membrane-mimetic environment, *Biochemistry 42*, 10311−10323.
79. Wegener K. L., Carver J. A., and Bowie J. H. (2003) The solution structures and activity of caerin 1.1 and caerin 1.4 in aqueous trifluoroethanol and dodecylphosphocholine micelles, *Biopolymers 69*, 42−59.
80. Balla M. S., Bowie J. H., and Separovic F. (2004) Solid-state NMR study of antimicrobial peptides from Australian frogs in phospholipid membranes, *Eur. Biophys. J. 33*, 109−116.
81. Thompson, J. D., Gibson, T. J., Plewniak, F., Jeanmougin, F., and Higgins, D. G. (1997) The CLUSTAL X windows interface: Flexible strategies for multiple sequence alignment aided by quality analysis tools, *Nucleic Acids Res. 24*, 4876−4882.
82. Wishart, D. S., Bigam, C. G., Holm, A., Hodges, R. S., and Sykes, B. D. (1995) ^{1}H, ^{13}C, and ^{15}N random coil NMR chemical shifts of the common amino acids. I. Investigations of nearest-neighbor effects, *J. Biomol. NMR 5*, 67−81.
83. Wishart, D. S., Sykes, B. D., and Richards F. M. (1991) Relationship between nuclear magnetic resonance chemical shift and protein secondary structure, *J. Mol. Biol. 222*, 311−333.

BI051711I